Annealing effects on the chemical configuration of uncapped and (poly-Si)-capped HfOxNy film deposited on Si(001)

Couillard, M.; Lee, M. -S.; Landheer, D.; Wu, X.; Botton, G. A.

Publisher's version / Version de l'éditeur:
https://doi.org/10.1149/1.1939087
Journal of the Electrochemical Society, 152, 8, pp. F101-F106, 2005

Journal of The Electrochemical Society, **152** (8) F101-F106 (2005)
0013-4651/2005/152(8)/F101/6/$7.00 © The Electrochemical Society, Inc.

Annealing Effects on the Chemical Configuration of Uncapped and (Poly-Si)-Capped HfO_xN_y Films Deposited on Si(001)

M. Couillard,[a] M.-S. Lee,[b] D. Landheer,[c,*] X. Wu,[c] and G. A. Botton[a,z]

[a]*Brockhouse Institute for Materials Research, McMaster University, L8S 4M1 Hamilton, Canada*
[b]*Department of Materials Science and Engineering, University of Toronto, M5S 3E4 Toronto, Canada*
[c]*Institute for Microstructural Sciences, National Research Council of Canada, K1A 0R6 Ottawa, Canada*

We use spatially resolved spectroscopy in a scanning transmission electron microscope to study the thermal stability of the HfO_xN_y/Si(001) system with and without an *in situ* capping layer of silicon. The films were deposited by metallorganic chemical vapor deposition using the amide precursor tetrakis(diethylamido)hafnium with NO as the oxidant. A SiO_xN_y interfacial layer (~1.8 nm) is observed at the HfO_xN_y/substrate interface for films directly exposed to air. In addition, the N loss in the HfO_xN_y film for the uncapped sample is significant. In contrast, *in situ* capping is found to reduce the thickness of the interfacial layer and to keep the N content in the final dielectric film high. The capped HfO_xN_y films are quasi-amorphous, whereas uncapped films are polycrystalline following exposure to air. Oxinitridation at both interfaces is observed following a rapid thermal annealing process (900°C in N_2 for 30 s) of the capped HfO_xN_y film. However, the interfacial layers remain thin (~1 nm) and a significant amount of N is present in the HfO_xN_y film. The rapid thermal annealing leads to the partial crystallization of the HfO_xN_y film and the Si capping layer. No Hf silicate is detected on a scale of ~6 Å in the electron energy loss spectroscopy analysis.
 [DOI: 10.1149/1.1939087]

Manuscript submitted November 22, 2004; revised manuscript received February 16, 2005. Available electronically July 7, 2005.

Hafnium oxide (HfO_2) has been proposed as an alternative high-*k* dielectric to SiO_2 for future complementary metal-oxide-semiconductor (CMOS) devices.[1] However, HfO_2 thin films have a low crystallization temperature[2,3] and a high oxygen permeability,[4] which causes the formation of a detrimental SiO_2 layer at the Si substrate interface when the dielectric film is exposed to air. In addition, there is a concern about the possible formation of Hf silicate and silicide at the interfaces.[5] Recently, the addition of N to form HfO_xN_y films has been proposed to improve stability.[6-10] The presence of N has been found to reduce the growth of the interfacial layer and to raise the crystallization temperature.[6] Furthermore, a study on HfO_xN_y gate dielectrics prepared by reactive sputtering reported an improved thermal and electrical stability, which was attributed to Si-N bonds at the interface with the substrate.[8] However, recent results have indicated that oxidation can result in a significant loss of N in the HfO_xN_y films.[10] Oxidation can be avoided if the dielectric film is capped with a material that prevents the diffusion of oxygen[11-13]; hence, a capping layer may prevent the replacement of N in HfO_xN_y by O from the atmosphere. The compatibility of the high-*k* film with the capping layer remains an important issue,[14] and the chemistry of the gate stack, especially at the interfaces, needs to be explored. In particular, understanding the influence of capping and annealing on the distribution of N is essential for the incorporation of nitrated high-*k* films in CMOS fabrication.

The characterization in this experiment has been performed with high-resolution transmission electron microscopy (HR-TEM) along with spatially resolved spectroscopy and high-angle annular dark-field (HAADF) imaging in a scanning TEM (STEM). Depth profiles of elements are obtained from the simultaneous collection in STEM mode of signals from electron energy loss spectroscopy (EELS) and energy-dispersive X-ray spectroscopy (EDS). Moreover, EELS analysis of the energy loss near-edge structures (ELNES), which provide information on the surrounding of excited atoms, allows the mapping of phases rather than just elements. EELS has previously been applied to the study of several high-*k* films, including HfO_2,[15] Gd_2O_3,[16] Sc_2O_3,[17] Y_2O_3,[12] La_2O_3,[18] Al_2O_3,[19] Hf silicate,[20] Zr silicate,[21] and Gd and La silicate.[22] In the EELS-STEM approach, the analysis region for a profile is directly selected from a high-resolution HAADF-STEM image, which provides contrast based on the atomic number. The local chemical and electronic information extracted from simultaneously recorded spectra of EELS and EDS can be correlated with the structural information contained in HAADF-STEM images.[23]

In this work, we investigate the stability of uncapped and (poly-Si)-capped HfO_xN_y films deposited on a Si(001) substrate by metallorganic chemical vapor deposition (MOCVD) using the amide precursor tetrakis(diethylamido)hafnium (TDEAH), $[(C_2H_5)_2N]_4Hf$ with NO as the oxidant. In particular, we trace the distribution of nitrogen and oxygen before and after a rapid thermal annealing (RTA) process. This study complements previous X-ray photoelectron spectroscopy (XPS) investigations on uncapped HfO_xN_y films.[6,24] The EELS analysis presented here confirms that the exposure of uncapped HfO_xN_y films to air leads to the oxinitridation of the substrate and the loss of N in the dielectric film. *In situ* capping is found to prevent oxidation of the sample and thus to reduce growth of the SiO_xN_y interfacial layer. The N content in capped HfO_xN_y films is also higher. RTA (900°C, in N_2 for 30 s) of the capped film results in oxinitridation of both the (HfO_xN_y/substrate) and the (HfO_xN_y/capping layer) interface. The diffusion of excess O and N in the dielectric films is thought to be responsible for this process. The resulting gate stack configuration, including the thin interfacial layers, is Si (substrate)/SiO_xN_y/HfO_xN_y/SiO_xN_y/Si (capping layer).

Experimental

p-Type Si(001) substrates with a resistivity of 0.035-0.065 Ω cm were given a HF-last RCA clean just prior to their introduction into an ultrahigh vacuum system, which comprises a low-pressure MOCVD chamber, an *in situ* XPS system, and a rapid postdeposition annealing (PDA) chamber. The vacuum system also contains a rod-fed electron-beam evaporator for the deposition of amorphous silicon films. For the deposition of the hafnium oxynitride films by MOCVD, a 0.1 M solution of TDEAH dissolved in octane was introduced with Ar carrier gas into the chemical vapor deposition (CVD) chamber with the vaporizer and gas distribution system held at 150°C. Si substrates were held at a temperature of 400°C during deposition, and the NO oxidant gas was introduced into the CVD chamber at a pressure of 11 mTorr through a separate gas introduction ring. The oxidant was introduced 5-10 min prior to film deposition with the substrate held at 500°C, for sample A, and at 400°C, for samples B and C. *In situ* XPS measurements confirm that for both temperatures a thin (~0.4 nm) buffer layer with equal concentrations of N and O forms on the Si substrate. They also show that this thickness saturates in 1-2 min and is not sensitive to oxi-

* Electrochemical Society Active Member.
z E-mail: gbotton@mcmaster.ca

Table I. Description of three processes included in the preparation of the three samples: the PDA, the *in situ* capping, and the RTA.[a]

Sample	PDA	*In situ* capping	RTA
A	800°C, 1 s, in vacuum	-	-
B	800°C, 1 s, in vacuum	~20 nm a-Si	-
C	800°C, 1 s, in vacuum	~20 nm a-Si	900°C, 30 s, in N_2

[a] A second capping layer of poly-Si (~200 nm) was deposited on sample B and C in a separate chamber before the RTA. The temperature of 600°C reached in the latter process partially crystallizes the first a-Si capping layer.

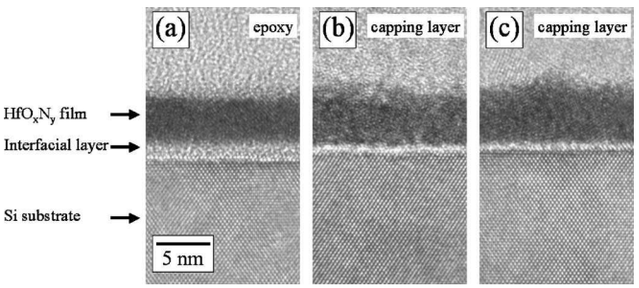

Figure 1. HR-TEM images for the three samples described in Table I: (a) A, (b) B, and (c) C.

dation time in the 5-10 min range. Separate precursor and oxidant pulses were employed during the deposition of ~5 nm thick films, with intervening nitrogen flushing steps to minimize carbon contamination. After deposition the films were transferred in ultrahigh vacuum (UHV) to the PDA chamber and annealed for 1 s at 800°C while the pressure remained $< 10^{-7}$ Torr. The capping of the dielectric films for sample B and C was carried out after the PDA in two steps. First, following the anneal, ~20 nm of amorphous Si was deposited *in situ* using the E-beam evaporator. The samples were then taken out of vacuum at room temperature and a further ~200 nm of poly-Si was deposited in a separate chamber using low-pressure CVD (LPCVD) at 600°C. The temperature reached in the latter process partially crystallized the a-Si layer initially deposited. For sample C, a further RTA was carried out at 900°C for 30 s in N_2 atmosphere.

The TEM characterization was carried out with a JEOL 2010F TEM/STEM with a Schottky field emission gun and operated at 200 keV. The microscope is equipped with a Gatan Tridiem energy filter and an Oxford Instruments (atmospheric thin window) EDS. The cross-section samples A, B, and C (see Table I) were prepared by tripod polishing[25] and low-energy (2 keV) ion milling. The images and the profiles were acquired with the Si substrate oriented along the ⟨110⟩ plane. The HAADF imaging and the spatially resolved spectroscopy were performed with a STEM probe size of approximately 2-3 Å. The angle of convergence was 10 mrad and the acceptance angle was 50 mrad for both HAADF imaging and EELS.

The chemical characterization was performed by simultaneously collecting the signals from EELS and EDS while the probe was scanned across the interfaces and the dielectric film. DigitalMicrograph software from Gatan was used for the EELS acquisition and also the EDS acquisition through an interface with Inca software from Oxford Instruments. The sampling for all the profiles is between 0.2 and 0.8 nm, and the acquisition time varied between 1 and 4 s. A small spatial drift was observed and corrected by assuming a constant rate and direction, which were deduced from HAADF images taken before and after the spectra recording. The drift-corrected linescan was then converted to a depth profile normal to the gate stack. In the EDS spectrum, the Si *K*-peaks and the Hf *M*-peaks overlap; and the signal for each element was extracted using a multiple linear least-squares (MLLS) fit of reference spectra obtained from principal component analysis (PCA). The MLLS fitting was performed with the routine available in the DigitalMicrograph environment. For the PCA, the eigenvectors were obtained from MatLab routines and a spectrum image was reconstructed following the method described in Ref. 26, which was implemented in the DigitalMicrograph environment. In EELS spectra, the background subtraction was performed with a power-law function extrapolated from the pre-edge region. The extraction of the N *K* edge (401 eV) signal was rendered more difficult by the presence of the Hf $N_{2,3}$ edge (380 eV) and was therefore performed using a 10 eV background window before the N *K* edge onset and a second background window just before the O *K* edge (~532 eV) onset.

Results and Discussion

HR-TEM images (Fig. 1) for the samples with deposition conditions summarized in Table I clearly show the difference in the thickness of the interfacial layer, which is estimated to be around 1.8 nm for sample A (Fig. 1a), 0.8 nm for sample B (Fig. 1b) and 1 nm for sample C (Fig. 1c). For the uncapped sample, the exposure to air led to the formation of a relatively thick interfacial layer. The growth of the interfacial layer has previously been attributed to the diffusion of atomic oxygen through the dielectric films. The diffusion of O is rate-limited and slows down with the growing interfacial layer.[27] *In situ* capping of the HfO_xN_y film reduces the thickness of the interfacial layer. Figure 1 also shows that the top interface of the capped HfO_xN_y films is rough. A first inspection indicates that the images of the capped dielectric film (sample B) do not show clear periodicity, but the speckle is not fully uniformed as expected for amorphous layers. We therefore associate the structure to what has been labeled quasi-amorphous.[15] In contrast, the uncapped film (sample A) is polycrystalline. Thus, the exposure to air at room temperature rather than the PDA process appears responsible for the partial crystallization of the uncapped HfO_xN_y film. The RTA in N_2 atmosphere of the capped dielectric film (Fig. 1c, sample C) induces the partial crystallization of both the HfO_xN_y film and the Si capping layer.

Figure 2 shows elemental profiles for the three samples. The profiles of Hf and O have been normalized to their maximum value. The N profiles have been normalized with respect to O using cross sections calculated from the Hartree-Slater model. The N distribution for sample A peaks inside the SiO_xN_y interfacial layer and the quantity of N remaining in the HfO_xN_y film is low. The element profiles of Fig. 2b indicate that most of the N remains inside the capped HfO_xN_y film. Moreover, the profiles show that the total N/O ratio is higher for sample B than for sample A. By preventing the exposure of the film to air, the capping layer suppresses the absorption and diffusion of O impurities from the ambient and by consequence reduces the interfacial SiO_xN_y growth. The observed interfacial layer for sample B (Fig. 2b) may be due partly to the formation of a buffer layer from the NO oxidant introduced prior to the precursor and partly because of migration during the PDA process of excess N and O contained in the dielectric film.

The profile for sample C (Fig. 2c) displays a reduction in the N and O intensity near the center of the HfO_xN_y film. Such a reduction in elemental profiles extracted from EELS can sometimes be attributed to layers containing heavy elements.[23] In our case, however, the ratio of the thickness t over the mean-free path λ taken on the Si substrate is lower for the profiles of Fig. 2c ($t/\lambda \sim 0.4$) than for Fig. 2b ($t/\lambda \sim 0.7$). Thus, the reduction in intensity would have been more pronounced for the profiles of Fig. 2b. We therefore associate the reduction in signal to the migration during the RTA process (900°C in N_2 for 30 s) of excess N and O in the HfO_xN_y film toward the interfaces. Moreover, the N/O ratio taken at the center of the HfO_xN_y film is lower for sample C than for sample B, implying that more N atoms than O atoms have diffused. The ox-

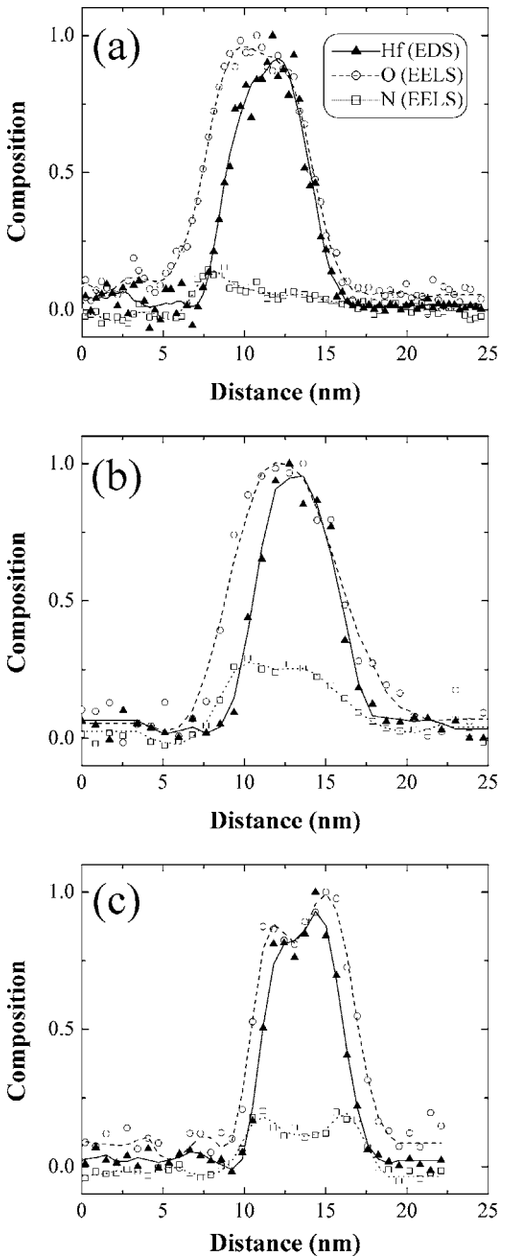

Figure 2. Elemental profiles for the three samples described in Table I: (a) A, (b) B, and (c) C. The Hf and O profiles are normalized with their maximum value equal to 1. The N profile is normalized with respect to O using inelastic (atomic) cross sections calculated from the Hartree-Slater model. The Si substrate is located on the left.

initridation of both interfaces (with the substrate and the capping layer) is also confirmed below in the analysis of the near-edge structure obtained by EELS.

Figure 3a shows a HAADF-STEM image for sample A. The interfacial layer appears as a darker band between the HfO_xN_y film and the substrate. Oxygen *K* edges from EELS spectra are presented in Fig. 3b for the HfO_xN_y film (top) and the SiO_xN_y interfacial layer (bottom) phases. The onset and the shape of the edge for the two phases are distinct. The profile of phases shown in Fig. 3c is obtained from a MLLS fit of the experimental spectra at each STEM probe position to the reference spectra of Fig. 3b. The profiles of HfO_xN_y and SiO_xN_y phases (top) are consistent with the elemental profiles (bottom). The comparison of the profiles also indicates that the ratio of N and O appears not to be uniform in both HfO_xN_y and SiO_xN_y. Changes in the ELNES of the O *K* edge in the oxynitride layer as a function of the N content, however, could not be detected within the energy resolution available to our system.

The EELS spectra for the Si $L_{2,3}$ edge shown in Fig. 4a were taken from sample A on the Si substrate (top) and the interfacial layer (bottom). The onset of the near-edge structure at the interfacial layer is located at lower energy than for SiO_2 and at higher energy than for Si_3N_4.[28] The position of the onset is explained by the presence of both N and O atoms as the first neighbors of Si atoms. This confirms that the interfacial layer is silicon oxynitride. Figure 4b illustrates the profiles for pure Si (substrate) and SiO_xN_y obtained for a MLLS fit to the reference spectra of Fig. 4a. The profiles focus on the interface between the substrate and the interfacial layer; the HfO_xN_y film is located on the right (outside the profile). An additional component extracted with PCA using the method described in Ref. 26 shows a structure at the Si/SiO_xN_y interface. The variation of the Si ELNES at this interface is associated mainly with a change in stoichiometry but may also be influenced by a possible change in the N/O ratio near the interface.

For the capped HfO_xN_y film (sample B), the O *K* near-edge analysis confirms the presence of a SiO_xN_y layer at the (HfO_xN_y/substrate) interface. A second SiO_xN_y layer at the (HfO_xN_y/capping layer) interface is also revealed, but only in some of the phase profiles. The elemental profile of Fig. 2b is consistent with the presence of a second interfacial layer, because the O distribution extends into the poly-Si capping layer (located to the right of the HfO_xN_y film in the profile). The absence of the second interfacial layer in some profiles can be explained either by a low signal extracted from the MLLS fits (*i.e.*, below the noise level) or to the nonuniform nature of the second SiO_xN_y layer. The latter possibility is consistent with the rough (HfO_xN_y/capping layer) interface. However, the morphology of the second interfacial layer has not been fully characterized.

A HAADF-STEM image of a capped HfO_xN_y film following RTA is shown in Fig. 5a. The elemental profiles for sample C (Fig. 5b) show that both N and O have migrated away from the HfO_xN_y film. The phase mapping of Fig. 5b confirms the oxynitridation at the interfaces with both the Si substrate and the Si capping layer. The resulting configuration is therefore present: Si (substrate)/SiO_xN_y/HfO_xN_y/SiO_xN_y/Si (capping layer). For Fig. 5b, the Si $L_{2,3}$ edge (~99 eV) and the O *K* edge (~532 eV) were included in the same EELS acquisition, allowing the simultaneous ELNES mapping of pure Si (with the Si $L_{2,3}$ edge), SiO_xN_y (with both the Si $L_{2,3}$ edge and the O *K* edge), and HfO_xN_y (with the O *K* edge). Because the SiO_xN_y interfacial layer was too thin, the reference spectra for the MLLS fit were taken from sample A for the O *K* edge (Fig. 3b) and for the Si $L_{2,3}$ edge (Fig. 4a). The C *K* edge (~284 eV) was also included in the same acquisition. Although it is possible that some carbon from the precursor remains in the dielectric film,[29] we could not detect any evidence of Hf-C bonds using PCA. For sample C, the shape of the Si $L_{2,3}$ edge taken at the capping layer is very similar to the one at the substrate. This is in contrast to sample B, where due to the smaller grain size in the gate, a broader first peak (99 eV) in the Si $L_{2,3}$ edge is detected. The results confirm the HR-TEM observations (Fig. 1) indicating that the RTA has induced partial crystallization of the capping layer.

Principal component analysis of the O *K* and the Si $L_{2,3}$ edges indicates that the samples included no detectable amount Hf silicate (or silicide) on the length scale of ~6 Å. A previous study on the (poly-Si)-capped HfO_2/Si system also found, with a similar approach, no detectable Hf silicate intermixing.[15] Because of the difference between the O *K* edge of HfO_2 and Hf silicate ($HfSiO_4$),[30] the presence of silicate would show up as a structured residual in the MLLS fits or as an additional significant component in PCA. The significant drop of the Si signal (extracted from EELS) in the HfO_xN_y film supports the finding that no silicate is present. The

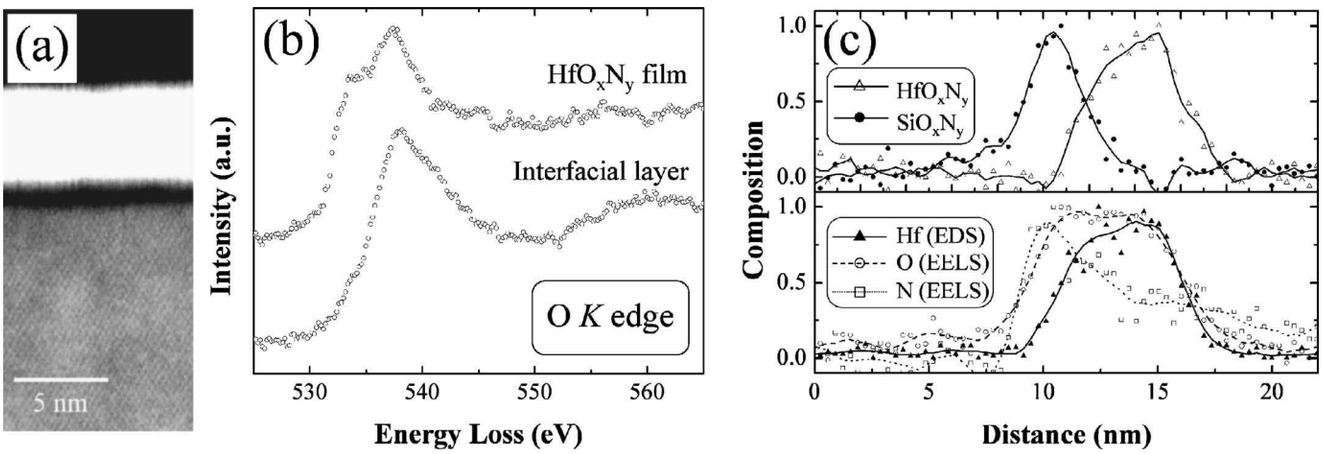

Figure 3. (a) HAADF-STEM image of an uncapped HfO_xN_y film (sample A, see Table I). (b) O *K* near-edge structure for the HfO_xN_y film (top) and the interfacial layer (bottom). (c) Phase profiles (top) of HfO_xN_y and SiO_xN_y, and elemental profiles (bottom) of Hf, O, and N. All profiles are normalized with their maximum value equal to 1 and the Si substrate is located on the left.

formation of silicate has previously been detected in HfO_2/Si systems.[31] However, in that case, the oxidation occurred after sputter deposition of Hf. The substrate temperature and the oxygen pressure during oxidation of Hf film have been found to be critical for the interfacial reactions, especially for silicate formation.[32] In Ref. 31, the presence of a nitrided layer on the Si substrate was found to reduce (without preventing) the intermixing. In our case, the introduction of the NO oxidant gas prior to the Hf precursor creates a nitrided layer on the Si substrate. Moreover, the oxidation of the Hf film occurs during each cycle, which consists of (N_2, NO, N_2, precursor) pulses. These growth conditions appear to prevent the formation of silicate.

The distribution of N in the gate stack, especially following necessary processing steps such as RTA, is critical to define the dielectric properties. The source of N in our sample preparation is from both the NO oxidant gas and the precursor. For the uncapped sample, a significant loss of N in the HfO_xN_y film is observed and a relatively thick SiO_xN_y interfacial layer is formed at the substrate interface. Similar observations were made on HfO_xN_y gate dielectrics prepared by reactive sputtering.[10] The loss of N in the film and the oxinitridation of the interfacial layer are attributed to the incorporation of O in the film in exchange of O and N. Such a process was clearly demonstrated for AlON films, where annealing in $^{18}O_2$ led to the incorporation of ^{18}O in replacement for ^{16}O and N previously existing in the film.[33] For capped samples, oxinitridation occurs for both the substrate and the capping layer, but the resulting interfacial layers are thinner than for uncapped samples. Furthermore, no significant oxidation occurs and thus the total N/O ratio remains high.

In Ref. 15, an unintentional SiO_2 layer was observed at the top interface of a HfO_2 film capped with a poly-Si electrode. The addition of a nitrided layer between the HfO_2 and the poly-Si was proposed as a solution to this reaction layer. The N-Si bonds formed at a HfO_xN_y/Si interface were identified as a factor leading to an increased thermal and electrical stability of high-*k* films.[7] In addition, SiO_xN_y has a slightly higher dielectric constant than SiO_2 and the growth of a SiO_xN_y layer is slower.[34] Experiments where nitridation of the surface was performed prior to film deposition have also demonstrated that the incorporation of N produces a diffusion barrier.[31,35] However, the observed SiO_xN_y layer at the (HfO_xN_y/capping layer) interface is not as well defined as the interfacial layer at the (HfO_xN_y/substrate) interface. The instability at the interface may therefore critically affect the use of poly-Si in a first generation gate.

For capped samples, a large quantity of N remains inside the HfO_xN_y film, even after RTA (Fig. 5c). The low availability of O to replace N in the dielectric films explains this result. We note how-

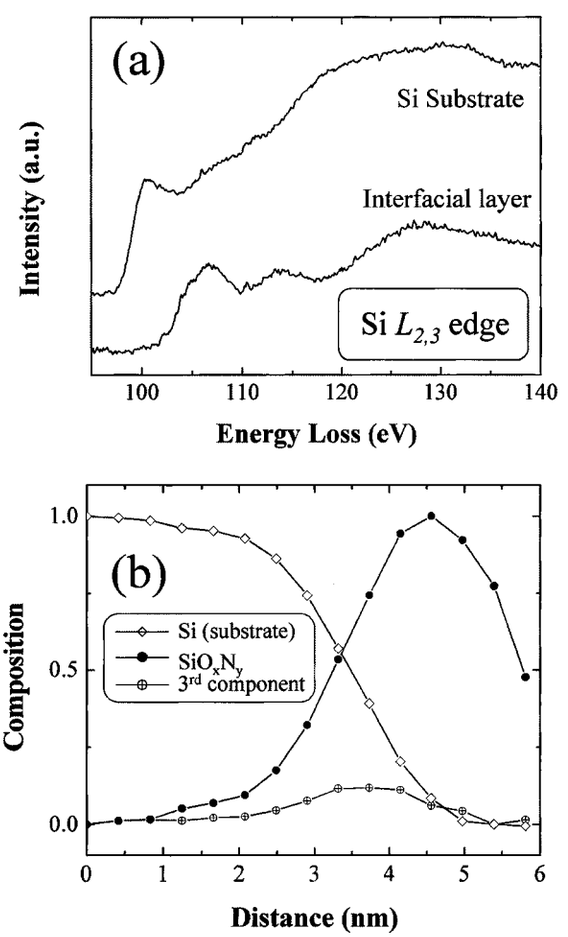

Figure 4. (a) Si $L_{2,3}$ edge for the substrate (top) and the interfacial layer (bottom) obtained from sample A (see Table I). (b) Phase profiles of pure Si and SiO_xN_y. An additional component extracted from PCA is also included in (b).

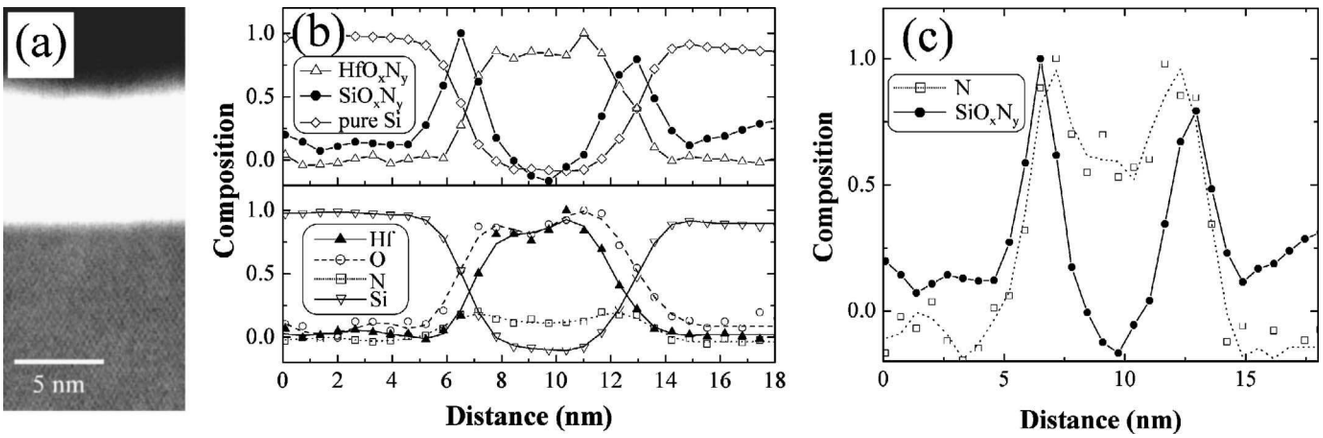

Figure 5. (a) HAADF-STEM image of a capped HfO_xN_y/Si sample following RTA (sample C, see Table I). (b) Phase profiles (top) and elemental profiles (bottom). The signal for N, O, and Si was extracted from EELS and the signal for Hf was extracted from EDS. (c) Profile of N and SiO_xN_y. The N profile in (b) is normalized with respect to O using inelastic (atomic) cross sections calculated from the Hartree-Slater model. Other profiles are normalized with their maximum value equal to 1. The Si substrate is located on the left in the profiles.

ever that a small quantity of residual O in the RTA chamber might have diffused through the gate and replaced some N in the dielectric film. N has the effect of decreasing the mean Hf coordination in HfO_xN_y.[9] This is in contrast with SiO_xN_y, where N increases the mean Si coordination. This difference has been explained.[9] by the fact that N tends to be in fourfold coordination when bonded to Hf, whereas it is threefold when bonded to Si. The authors of Ref. 9 associate the reduction in Hf coordination to HfO_xN_y being a better glass former and therefore having a higher crystallization temperature than HfO_2. Furthermore, the presence of N in high-*k* oxide films also reduces the diffusion of impurities through the film.

Conclusions

In summary, HfO_xN_y films were deposited on Si(001) by MOCVD using $[(C_2H_5)_2N]_4Hf$ with NO as the oxidant. The stability of both uncapped and (poly-Si)-capped films was investigated. The local chemistry, in particular the nitrogen distribution, and the bonding environment of atoms were determined with spatially resolved EELS and EDS collected simultaneously with a subnanometer resolution. The exposure of HfO_xN_y films to air results in the replacement of nitrogen in the film by oxygen and in the formation of a SiO_xN_y layer ($\sim$1.8 nm) at the near interface with the Si substrate. The elemental profiles also suggest that the N/O ratio is not uniform across the HfO_xN_y film and the SiO_xN_y interfacial layer. HR-TEM imaging indicates that the uncapped HfO_xN_y film is polycrystalline.

In contrast, no oxidation is detected for HfO_xN_y films capped in vacuum. The (poly-Si)-capped dielectric film retains a significant quantity of nitrogen and the thickness of the oxinitride interfacial layer is much reduced. Thus, *in situ* capping is found to be necessary and efficient to control the interface composition. Furthermore, the HfO_xN_y film remains quasi-amorphous. An RTA (900°C in N_2 for 30 s) of the capped dielectric film results in the migration of nitrogen and, to a lesser extent, oxygen away from the film, leading to the oxinitridation of both interfaces with silicon (substrate and capping layer). However, the interfacial layers remain thin, which crucially affects the overall capacitance of the system. The presence of the nitrided layer between the high-*k* films and the silicon is expected to be beneficial for the stability of the gate stack by acting as a diffusion barrier for different species (*e.g.*, O, Si, B). The N content in the capped high-*k* films, even following RTA, remains high. A higher crystallization temperature and reduced diffusion of impurities is therefore expected. However, the capped film following RTA is polycrystalline, and further studies on the morphology of the film are needed. Further work on the electrical properties of the resulting gate stack of Si (substrate)/SiO_xN_y/HfO_xN_y/SiO_xN_y/Si (capping layer) is also required.

Acknowledgment

The authors thank NSERC for financial support of this work. They are grateful to Fred Pearson and Andy Duft for technical support and maintenance of the facilities. One of the authors (M.C.) acknowledges support from an NSERC fellowship. Facilities are supported by NSERC, Canada Foundation for Innovation and Ontario Innovation Trust.

McMaster University assisted in meeting the publication costs of this article.

References

1. G. D. Wilk, R. M. Wallace, and J. M. Anthony, *J. Appl. Phys.*, **89**, 5243 (2001).
2. H. Kim, P. C. McIntyre, and K. C. Saraswat, *Appl. Phys. Lett.*, **82**, 106 (2003).
3. M.-Y. Ho, H. Gong, G. D. Wilk, B. W. Busch, M. L. Green, P. M. Voyles, D. A. Muller, M. Bude, W. H. Lin, A. See, M. E. Loomans, S. K. Lahiri, and P. I. Räisänen, *J. Appl. Phys.*, **93**, 1477 (2003).
4. A. S. Foster, A. L. Shluger, and R. M. Nieminen, *Phys. Rev. Lett.*, **89**, 225901 (2002).
5. S. Stemmer, *J. Vac. Sci. Technol. B*, **22**, 791 (2004).
6. M. Lee, Z.-H. Lu, W.-T. Ng, D. Landheer, X. Wu, and S. Moisa, *Appl. Phys. Lett.*, **83**, 2638 (2003).
7. K.-J. Choi, J.-H. Kim, and S.-G. Yoon, *J. Electrochem. Soc.*, **151**, G262 (2004).
8. C. S. Kang, H.-J. Cho, K. Onishi, R. Nieh, R. Choi, S. Gopalan, S. Krishnan, J. H. Han, and J. C. Lee, *Appl. Phys. Lett.*, **81**, 2593 (2002).
9. G. Shang, P. W. Peacock, and J. Robertson, *Appl. Phys. Lett.*, **84**, 106 (2004).
10. J. F. Kang, H. Y. Yu, C. Ren, M.-F. Li, D. S. H. Chan, H. Hu, H. F. Lim, W. D. Kang, D. Gui, and D.-L. Kwong, *Appl. Phys. Lett.*, **84**, 1588 (2004).
11. B. W. Busch, J. Kwo, M. Hong, J. P. Mannaerts, B. J. Sapjeta, W. H. Schulte, E. Garfunkel, and T. Gustafsson, *Appl. Phys. Lett.*, **79**, 2447 (2001).
12. S. Stemmer, D. O. Klenov, Z. Chen, D. Niu, R. W. Ashcraft, and G. N. Parsons, *Appl. Phys. Lett.*, **81**, 712 (2002).
13. M. Kundu, N. Miyata, T. Nabatame, T. Horikawa, M. Ichikawa, and A. Toriumi, *Appl. Phys. Lett.*, **82**, 3442 (2003).
14. D. C. Gilmer, R. Hegde, R. Cotton, R. Garcia, V. Dhandapani, D. Triyoso, D. Roan, A. Franke, R. Rai, L. Prabhu, C. Hobbs, J. M. Grant, L. La, S. Samavedam, B. Taylor, H. Tseng, and P. Tobin, *Appl. Phys. Lett.*, **81**, 1288 (2002).
15. G. D. Wilk and D. A. Muller, *Appl. Phys. Lett.*, **83**, 3984 (2003).
16. G. A. Botton, J. A. Gupta, D. Landheer, J. P. McCaffrey, G. I. Sproule, and M. J. Graham, *J. Appl. Phys.*, **91**, 2921 (2002).
17. G. A. Botton, E. Romain, D. Landheer, X. Wu, M.-Y. Wu, M. Lee, and Z.-H. Lu, in *Silicon Nitride and Silicon Dioxide Thin Insulating Films*, R. E. Sah, K. B. Sundaram, M. J. Deen, D. Landeer, W. D. Brown, and D. Misra, Editors, PV 2003-02, p. 251, The Electrochemical Society Proceedings Series, Pennington, NJ 2003).
18. S. Stemmer, J.-P. Maria, and A. I. Kingon, *Appl. Phys. Lett.*, **79**, 102 (2001).
19. R. F. Klie, N. D. Browning, A. R. Chowdhuri, and C. G. Takoudis, *Appl. Phys. Lett.*, **83**, 1187 (2003).
20. N. Ikarashi, M. Miyamura, K. Masuzaki, and T. Tatsumi, *Appl. Phys. Lett.*, **84**, 3672 (2004).
21. D. A. Muller and G. D. Wilk, *Appl. Phys. Lett.*, **79**, 4195 (2001).

22. X. Wu, D. Landheer, T. Quance, M. J. Graham, and G. A. Botton, *Appl. Surf. Sci.*, **200**, 15 (2002).
23. B. Foran, J. Barnett, P. S. Lysaght, M. P. Agustin, and S. Stemmer, *J. Electron Spectrosc. Relat. Phenom.*, In press.
24. M. Lee, D. Landheer, X. Wu, M. Couillard, Z.-H. Lu, and W.-T. Ng, *Mater. Res. Soc. Symp. Proc.*, **811**, 7.2.1 (2004).
25. P. M. Voyles, J. L. Grazul, and D. A. Muller, *Ultramicroscopy*, **96**, 251 (2003).
26. N. Bonnet, N. Brun, and C. Colliex, *Ultramicroscopy*, **77**, 97 (1999).
27. B. W. Busch, W. H. Schulte, E. Garfunkel, T. Gustafsson, W. Qi, R. Nieh, and J. Lee, *Phys. Rev. B*, **62**, R13290 (2000).
28. K. Kimoto, K. Kobayashi, T. Aoyama, and Y. Mitsui, *Micron*, **30**, 121 (1999).
29. J. Schaeffer, N. V. Edwards, R. Liu, D. Roan, B. Hradsky, R. Gregory, J. Kulik, E. Duda, L. Contreras, J. Christiansen, S. Zollner, P. Tobin, B.-Y. Nguyen, R. Nieh, M. Ramon, R. Rao, R. Hegde, R. Rai, J. Baker, and S. Voight, *J. Electrochem. Soc.*, **150**, F67 (2003).
30. D. W. McComb, A. J. Craven, D. A. Hamilton, and M. MacKenzie, *Appl. Phys. Lett.*, **84**, 4523 (2004).
31. P. D. Kirsch, C. S. Kang, J. Lozano, J. C. Lee, and J. G. Ekerdt, *J. Appl. Phys.*, **91**, 4353 (2002).
32. J.-H. Lee, N. Miyata, M. Kundu, and M. Ichikawa, *Phys. Rev. B*, **66**, 233309 (2002).
33. K. P. Bastos, R. P. Pezzi, L. Miotti, G. V. Soares, C. Driemeier, J. Morais, I. J. R. Baumvol, C. Hinkle, and G. Lucovsky, *Appl. Phys. Lett.*, **84**, 97 (2004).
34. N. Bassim, V. Craciun, J. Howard, and R. K. Singh, *Appl. Surf. Sci.*, **205**, 267 (2003).
35. K. P. Bastos, J. Morais, L. Miotti, G. V. Soares, R. P. Pezzi, R. C. G. da Silva, H. Boudinov, I. J. R. Baumvol, R. I. Hegde, H.-H. Tseng, and P. J. Tobin, *J. Electrochem. Soc.*, **151**, F153 (2004).